

Sol-gel transition in heteroassociative RNA-protein solutions: A quantitative comparison of coarse-grained simulations and the Semenov-Rubinstein theory

Xinxiang Chen,^{1,*} Jude Ann Vishnu,¹ Pol Besenius,² Julian König,^{3,4} and Friederike Schmid^{1,†}

¹*Institute of Physics, Johannes Gutenberg-University, 55099 Mainz, Germany*

²*Department of Chemistry, Johannes Gutenberg-University, 55099 Mainz, Germany*

³*Institute of Molecular Biology, 55128 Mainz, Germany*

⁴*Theodor Boveri Institute, Biocenter, University of Würzburg, 97074 Würzburg, Germany*

Protein RNA-binding domains selectively interact with specific RNA sites, a key interaction that determines the emergent cooperative behaviors in RNA-protein mixtures. Through molecular dynamics simulations, we investigate the impact of the specific binding interactions on the phase transitions of an exemplary RNA-protein system and compare it with predictions of the Semenov-Rubinstein theory of associative polymers. Our findings reveal a sol-gel (percolation) transition without phase separation, characterized by double reentrant behavior as the RNA or protein concentration increases. We highlight the crucial role of bridge formations in driving these transitions, particularly when binding sites are saturated. The theory quantitatively predicts the binding numbers at equilibrium in the semidilute regime, but it significantly overestimates the size of the concentration range where percolation is observed. This can partly be traced back to the fact that the mean-field assumption in the theory is not valid in the dilute regime, and that the theory neglects the existence of cycles in the connectivity graph of the percolating cluster at the sol-gel transition. Our study enriches the understanding of RNA-protein phase behaviors, providing valuable insights for the interpretation of experimental observations.

I. INTRODUCTION

Phase transitions play a crucial role in maintaining the structural integrity and functional diversity of biological systems[1]. Currently, liquid-liquid phase separation (LLPS) is widely studied in cellular biophysics, especially with respect to its potential importance for the formation of membraneless organelles. The complex interplay of protein and RNA interactions leads to a diverse spectrum of phase behaviors governed by factors such as temperature, pH, salt conditions, and the molecular architecture[2]. Most research on LLPS has focused on protein phase separation and its role in organelle formation[3]. However, many cellular processes such as RNA splicing, transport, and stability, depend on the combined action of RNA and proteins[4–8].

While extensive research has been devoted to understanding phase separation in RNA-protein systems[9, 10], highlighting RNA’s ability to enhance phase separation alongside protein-protein interactions[11], gelation, which is another important cooperative phenomenon, has received much less attention. The sol-gel (percolation) transition describes the transformation of a liquid-like sol into a gel-like state, characterized by the formation of interconnected networks that span the entire system. Already in systems containing only proteins, gelation without phase separation has been observed, pointing at a complex interplay of molecular interactions[12, 13]. Introducing RNA into these systems adds another layer of complexity due to the asymmetry between RNA and protein components, resulting in an even wider spectrum of

phase behaviors[14, 15]. This highlights the necessity for more research into how specific RNA-protein interactions lead to the formation of structured networks.

The structural diversity of RNA and proteins – such as RNA’s linear sequences, complex tertiary structures, and proteins’ functional domains like intrinsically disordered regions (IDRs) and RNA-binding domains (RBDs) – plays a crucial role in shaping phase behavior. The solubility of proteins, often influenced by IDRs, and the binding specificity provided by RBDs, are important factors for the formation of condensates and gels [12, 16]. RBDs, in particular, determine how proteins interact with various RNA sequences, leading to the formation of different phase-separated structures[17, 18]. Different RNA species have been shown to induce different condensate properties in RNA-protein mixtures. For example, the interactions between Poly(A), Poly(U), and Poly(C) and proteins typically give rise to the formation of liquid-like droplets, whereas Poly(G)-protein mixtures form gel-like structures [19, 20]. Understanding the molecular origin of these different behaviors is thus essential for unraveling the complex cooperative phenomena observed in RNA-protein mixtures.

The interactions between the binding sites in RNA and proteins are traditionally classified as either specific or nonspecific [9, 11, 14, 21, 22]. Specific binding involves the interaction of RBDs in proteins with special sequences or motifs on RNA, whereas nonspecific binding enables proteins to interact with RNA sites lacking identifiable sequences or structural motifs. These interactions encompass a range of forces, including charge–charge, dipole–dipole, π – π , and cation– π interactions[23–26]. Electrostatics is often one of the key factors driving or controlling LLPS, but some studies have also identified phase transitions within complex biological sys-

* xichen@uni-mainz.de

† friederike.schmid@uni-mainz.de

tems that mostly rely on non-electrostatic interactions [12, 13, 27, 28].

To model such systems in molecular dynamics simulations, two prevailing approaches have emerged. Sticker-spacer models utilize "stickers" to mimic the multivalent binding domains on RNA or protein chains, which are connected by neutral domains called spacers [12, 27, 29, 30]. Alternatively, patchy-particle models treat each multivalent chain as a sphere with different kinds of anisotropic attractive patches on its surface [31, 32]. These two minimal models have proven effective in explaining the phase behavior of biological systems. In the patchy-particle models, one can control the number of patches on the surface of the particles to mimic the multivalent character. For example, Espinosa and coworkers have used a patchy particle model to demonstrate that higher valencies result in LLPS, and condensate formation is suppressed if the valency is 2 [31]. In the sticker-spacer models, multivalency is characterized by the number of stickers on a chain. Harmon and colleagues demonstrated the critical role of spacer solubility in influencing phase behavior [12]. They found that in associative polymers with the same structure, the explicit inclusion of spacers—occupying significant volume—prevents phase separation.

In the present study, we explore the cooperative effects that specific binding interactions induce in RNA-protein solutions. We focus on specific binding effects characterized by exclusive interactions between a sticker from RNA and a sticker from a protein, thereby preventing engagement with additional stickers. To this end, we consider an idealized minimal spring-bead model with beads that have no non-specific interactions apart from their excluded volume interactions. The emerging cooperative behavior in this model is studied using two different approaches: First, large-scale off-lattice molecular dynamics simulations, and second, an extension of the Semenov-Rubinstein theory of percolation and phase separation [29] to asymmetric heteroassociative mixtures [33]. We find that specific binding may lead to percolation without phase separation, resulting in the formation of connected clusters spanning across the whole system. Moreover, our study reveals the possibility of double-reentrant sol-gel-sol transitions upon varying the concentrations of RNA and proteins, in agreement with theoretical expectations [33]. To gain insights into the percolation transitions, we quantify the frequency of different binding structures such as bridges, which are central for network formation, loops, and isolated bonds. A comparison between theoretical predictions and simulation results shows that the theory captures the phase behavior and fairly accurately predicts binding numbers, particularly at high concentrations in the semidilute regime. Nevertheless, the theory falls short in quantitatively predicting percolation threshold values and overestimates the size of the parameter region where the system is gelled.

II. MODEL AND METHODS

II.A Simulation

We model RNA molecules and proteins in good solvent using a sticker-spacer model. Specifically, we consider proteins with distinct functional motifs capable of associating with certain RNA sequences, mirroring the finite number of RNA-binding domains (RBDs) found in natural proteins. For instance, hnRNPH, an RNA-binding protein within the heterogeneous nuclear ribonucleoproteins family, possesses three RNA-binding motifs [34], which play a crucial role in modulating the structure of RNA G quadruplexes, as highlighted in recent studies [35, 36]. Inspired by this, the "proteins" in our simulation also contain 3 binding domains, and we will refer to them as trimers in the following. RNA molecules will be modeled as long spring-bead chains with several binding sites. Binding sites will be modeled as stickers, which are connected by purely repulsive spacer chains. A schematic cartoon of these chain structures is shown in Fig. 1. Blue and orange beads correspond to stickers in protein and RNA chains respectively. Yellow beads correspond to spacers, linking stickers along each chain. RNA and protein stickers can associate with each other, mimicking specific binding, but stickers of the same type repel each other. Moreover, each sticker can only associate with at most one other sticker.

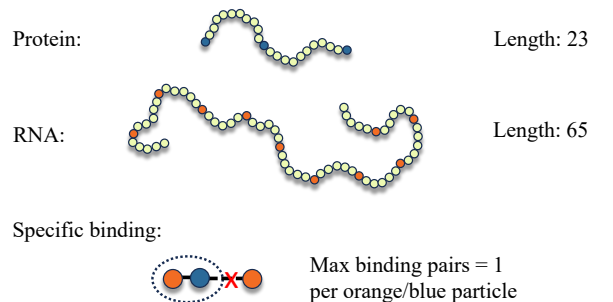


FIG. 1. Cartoon showing the model for RNA and protein in the present study. Blue, orange, and yellow beads are stickers in protein and RNA chains and spacers, respectively. To account for the specificity of binding interactions, each protein sticker is designed such that it can pair exclusively with a single RNA sticker.

Putting this more formally, we consider a system of n_A polymer chains A (RNA) n_B polymer chains B (proteins/trimers) in a volume V at temperature T . Polymers of type i ($i = A, B$) contain N_i monomers (beads), which includes f_i stickers that are evenly distributed along the chain. The mean monomer density of chains i is thus $c_i = n_i N_i / V$, and the mean density of i -stickers is $c_{si} = n_i f_i / V$. For simplicity, all monomers are taken to have the same mass m and diameter σ . Adjacent monomers in a chain are connected by a harmonic bond

potential:

$$\beta U_{\text{bond}} = \frac{1}{2} k_b (r - r_0)^2 \quad (1)$$

Here $\beta = 1/k_B T$ is the Boltzmann factor, k_b is the spring constant, $r_0 = \sqrt[6]{2} \sigma$ is the equilibrium bond length and σ is the diameter of the monomers as mentioned above, which serves as the length unit in our paper. Non-bonded pairs of monomers with the exception of pairs of A- and B-stickers interact via the purely repulsive Weeks–Chandler–Andersen (WCA) potential[37]:

$$\beta U_{\text{WCA}} = \begin{cases} 4\epsilon \left[\left(\frac{\sigma}{r}\right)^{12} - \left(\frac{\sigma}{r}\right)^6 + \frac{1}{4} \right] & r < \sqrt[6]{2}\sigma \\ 0 & r \geq \sqrt[6]{2}\sigma \end{cases}, \quad (2)$$

where ϵ is the interaction strength of the WCA potential. To emulate the specific binding between RNA and proteins, we incorporate a targeted interaction between A and B stickers. It ensures that a single A-sticker is capable of binding with just one B-sticker and vice versa, while any additional stickers are subject to exclusion through the WCA potential, as enforced by the already bound partner sticker. The specific binding potential is[38, 39]:

$$\beta U_{\text{binding}} = \begin{cases} -\epsilon_{\text{sp}} \left[\cos\left(\frac{2\pi r}{\sigma}\right) + 1 \right] & r < 0.5\sigma \\ 0 & r \geq 0.5\sigma \end{cases} \quad (3)$$

The strength of specific binding between stickers in RNA and trimers is controlled by ϵ_{sp} . In real RNA-protein systems, the RNA binding domains in proteins can link to RNA dynamically and reversibly through a weak chemical binding interaction, hence ϵ_{sp} can not be very large. Importantly, the specific binding potential's cut-off distance (0.5σ) combined with the purely repulsive interactions between homotypic monomers ensures the specificity of binding (see Fig. 1). The implementation of specific binding via a simple pairwise and isotropic attractive potential has distinct advantages from a computational point of view, because it can be implemented in a straightforward manner using standard optimized simulation packages. An alternative and arguably more natural way to mimic reversible directed binding between protein and RNA domains would be to implement reversible reactions, with Monte Carlo moves that satisfy detailed balance. Our model can capture this reversibility by controlling the binding process at the particle level through the competition between different interactions within the system.

We perform Langevin dynamics simulations with implicit solvent at a fixed temperature ($k_B T$ is the unit of energy), using the simulation package HOOMD-blue(version 2.9.3)[40]. The snapshots of our systems are visualized with OVITO[41]. The chain lengths of RNA and trimers are $N_A = 65$ and $N_B = 23$, respectively, and the number of stickers in each chain is $f_A = 10$ and $f_B = 3$. They are separated by spacers of length $l_A = 5$ and $l_B = 10$. The spring constant is set to

$k_b = 30k_B T/\sigma^2$, resulting in a statistical segment length of $a \approx 1.2\sigma$. We simulate the RNA-trimer system in a rectangular box ($100\sigma \times L_y \times 80\sigma$), in which the box size can be changed along the y -axis direction. The total duration of simulation runs is $10^6 t_0$ to make sure the system reaches the equilibrium state, with $t_0 = \sqrt{m\sigma^2/k_B T}$ being the time unit of the simulation. The strength of the WCA potential $\epsilon = 1 k_B T$. To specify ϵ_{sp} , we ran separate simulations of a system containing only one RNA and one trimer, and determined the average life time of specific binding as a function of ϵ_{sp} . The results are shown in Fig. 2. At $\epsilon_{\text{sp}} = 6k_B T$, we obtain $\tau \sim 10^3 t_0$, implying that the specific bonds can open and close frequently during one simulation run. Assuming that our simulation time unit corresponds to a real time span of the order of a picosecond, this lifetime scale aligns well with reversible binding events observed in real biological systems[42]. Therefore, in the following discussion, we keep $\epsilon_{\text{sp}} = 6k_B T$. Error bars on averaged quantities were estimated by computing the standard error of the mean.

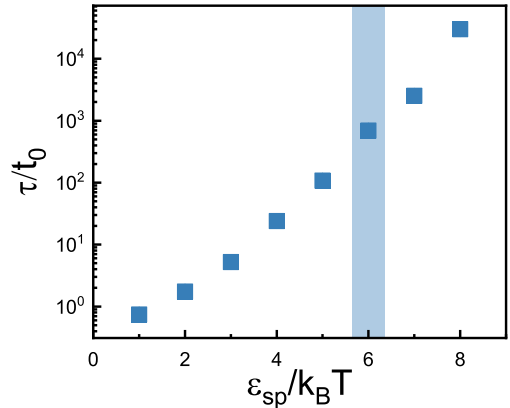


FIG. 2. The lifetime of specific binding for different binding strengths ϵ_{sp} , as obtained from simulations of one RNA and one trimer molecules, see text, in a small cubic box of side length 20σ .

II.B Theory

In Section III, we will compare the simulation results with the predictions of the Semenov-Rubinstein theory for reversible gelation in solutions of associative polymers [28, 29, 33, 43, 44]. Therefore, we now briefly recapitulate the central ideas of this mean-field approach and the main equations for the case of our particular system. We consider a two-component system of n_A and n_B chains with length N_A and N_B , each containing f_A or f_B stickers, in good solvent. A and B stickers can form reversible bonds, thereby gaining an energy ($-\epsilon_{\text{sp}}$) per bond. The mean-field approximation consists in neglect-

ing the correlations between sticker positions and chain conformations, such that the stickers behave like an ideal gas. This implies that the solution is semidilute in the sense that the spacers between stickers overlap, and that the influence of excluded volume interactions on sticker-sticker contacts can be neglected[29, 33]. It also implies that the chains are long and that the number of stickers per chain is high. The free energy per volume of the whole system is then composed of three parts:

$$\beta f = \beta f_{\text{entropy}} + \beta f_{\text{sticker}} + \beta f_{\text{int}}. \quad (4)$$

The first term is the pure translational entropy of polymer chains as a function of the monomer concentration $c_i = n_i N_i / V$:

$$\beta f_{\text{entropy}} = \frac{c_A}{N_A} \ln \left(\frac{c_A}{N_A e} \right) + \frac{c_B}{N_B} \ln \left(\frac{c_B}{N_B e} \right). \quad (5)$$

The second term, βf_{sticker} , is the free energy associated with the formation of reversible bonds between A - and B -stickers. For a given number N_p of bonds, it is calculated as follows:

$$\beta f_{\text{sticker}} = -\frac{1}{V} \ln \left[P_{\text{comb}} \left(\frac{v_b}{V} \right)^{N_p} e^{\beta \varepsilon_{\text{sp}} N_p} \right], \quad (6)$$

where v_b is the bond volume for specific binding and P_{comb} is the number of different ways how to distribute the N_p (AB) bonds onto $f_A n_A$ stickers of type A and $f_B n_B$ of type B :

$$P_{\text{comb}} = \binom{n_A f_A}{N_p} \binom{n_B f_B}{N_p} (N_p)!. \quad (7)$$

Using Stirling's approximation, Eq. (6) can be rewritten as

$$\begin{aligned} \beta f_{\text{sticker}} &= \frac{N_p}{V} + \frac{n_A f_A}{V} \ln(1 - p_A) + \frac{n_B f_B}{V} \ln(1 - p_B) \\ &\quad - \frac{N_p}{V} \ln \left[\frac{(n_A f_A - N_p)(n_B f_B - N_p)}{N_p} \frac{K^{-1}}{V} \right], \end{aligned} \quad (8)$$

in which $K = v_b^{-1} e^{-\beta \varepsilon_{\text{sp}}}$ is the dissociation constant. Here $p_i = N_p / n_i f_i$ ($i = A, B$) is the fraction of bound stickers for each component i .

The last term in Eq. (4) accounts for the excluded volume interactions between all monomers except A - and B -stickers,

$$f_{\text{int}} = \frac{1}{2} v [(c_A + c_B)^2 - 2c_{s_A} c_{s_B}], \quad (9)$$

which depends on the excluded volume parameter v and the i -sticker concentrations $c_{si} = n_i f_i / V = c_i f_i / N_i$ ($i = A, B$). In the following, we will characterize the system in terms of the sticker concentrations c_{si} instead of monomer concentrations c_i for convenience, and also introduce the total sticker concentration $c_s = c_{s_A} + c_{s_B}$. Minimizing the free energy with respect to N_p for given c_{si} we obtain

$$N_p = \frac{V}{2} (K + c_s - \sqrt{\Delta}), \quad (10)$$

$$\text{with } \Delta = (K + c_s)^2 - 4c_{s_A} c_{s_B},$$

which allows to calculate

$$p_i = N_p / n_i f_i = N_p / (c_{si} V), \quad (11)$$

and to derive the following expression for the free energy per area as a function c_{s_A}, c_{s_B} :

$$\begin{aligned} \beta f &= \frac{c_{s_A}}{f_A} \ln \left(\frac{c_{s_A}}{f_A e} \right) + \frac{c_{s_B}}{f_B} \ln \left(\frac{c_{s_B}}{f_B e} \right) \\ &\quad + c_{s_A} \left[\frac{p_A}{2} + \ln(1 - p_A) \right] \\ &\quad + c_{s_B} \left[\frac{p_B}{2} + \ln(1 - p_B) \right] \\ &\quad + \frac{1}{2} v \left[\left(\frac{c_{s_A} N_A}{f_A} + \frac{c_{s_B} N_B}{f_B} \right)^2 - 2c_{s_A} c_{s_B} \right]. \end{aligned} \quad (12)$$

Based on this expression, the stability and phase behavior of the system can be analyzed by standard methods. According to Danielsen *et. al.*[33], the underlying mean-field assumption is expected to become problematic if $vl > (a\sqrt{l})^3$, (excluded volume effects become important at the spacer level), and/or if $c_{si} < (a\sqrt{l})^{-3}$ for $i = A$ or B (spacers do not overlap), where l is the spacer length and a the statistical segment length.

Owing to the formation of specific bonds between polymers, the multivalent polymer chains can connect to a system-spanning network structure once the concentration reaches a certain threshold. This threshold for the sol-gel transition can be estimated using analytical approaches derived from the Flory-Stockmayer theory, which provides a basic understanding of polymer network formation and gelation processes[12, 28, 29, 45, 46]. Our system contains two different polymer components in solution. For each component i , the number of binding sites along one chain is f_i and the fraction of binding sites that are occupied is p_i .

We define clusters as sets of chains that are directly or indirectly connected to each other by specific bonds, and consider the thermodynamic limit $V \rightarrow \infty$. A gel is then characterized by the existence of an infinite cluster. A given chain of type i that is connected to a given cluster by one bond has, on average, $p_i(f_i - 1)$ additional bonds. Now let us consider a hypothetical algorithm that identifies clusters in a given configuration of (AB) bonds by reconstructing them in a stepwise fashion, starting from a single initial chain. In our system, A -stickers can only bind to B -stickers and vice versa. Thus an A chain that is connected to a partially reconstructed cluster via one B -chain has on average $p_A(f_A - 1)$ additional connections to B -chains, and these B -chains have on average $p_B(f_B - 1)$ additional connections to A -chains. Some of these connections will cycle back to the original partially reconstructed cluster. Thus, the A -chain in question has on average less than $m = p_A(f_A - 1)p_B(f_B - 1)$ B -mediated connections to "new" A -chains, i.e., chains that are not yet part of the original reconstructed cluster. In order to reconstruct an infinite cluster, m must necessarily exceed one. In the Rubinstein-Semenov theory [29, 33], the possibility of cycles is neglected and it is assumed that every

additional connection truly extends the size of the reconstructed cluster. In this case, we expect the percolation transition at

$$m = (f_A - 1)p_A \times (f_B - 1)p_B \stackrel{\dagger}{=} m_p = 1. \quad (13)$$

We emphasize that this condition is independent of the way how the p_i has been obtained. It is derived based on the assumption that graphs are tree-like, without accounting for specific molecular characteristics of the particular system. The threshold predicted by this equation only depends on the sticker number f_i and binding probability p_i . Therefore, the criterion must be seen as a rigorous lower bound for the value of m at the percolation threshold for given p_i . The true threshold value will be higher.

III RESULTS AND DISCUSSION

III.A Stability of the homogeneous system

In the exploration of the behavior of the RNA-trimer system, we begin with investigating the stability of the homogeneous system. This is first done analytically using the theory described above. Within this theory, a homogeneous mixture is (meta)stable if the Hesse matrix of the free energy per volume f (Eq. (12)) as a function of c_{s_A} and c_{s_B} , $H_{f;ij} = \partial^2 f / \partial c_{si} \partial c_{sj}$, is positive definite. The diagonal elements of the Hesse matrix are given by

$$\frac{\partial^2 \beta f}{\partial c_{si}^2} = p_i / \sqrt{\Delta} + v(N_i/f_i)^2 + 1/(f_i c_{si}) > 0, \quad (14)$$

(using the definitions of Eq. (10)) and always positive. However, the determinant may become negative. In the extreme case of very strong binding ($K \rightarrow 0$) and zero excluded volume interactions ($v = 0$), the determinant takes the value

$$\det(H_f)|_{v=0, K \rightarrow 0} = \frac{1}{c_{s_A} c_{s_B}} \times \left[\frac{1}{f_A f_B} - \frac{1 - \frac{1}{f_A} - \frac{1}{f_B}}{2} \left(\frac{c_s}{|c_{s_A} - c_{s_B}|} - 1 \right) \right]. \quad (15)$$

This result shows that the homogeneous state necessarily becomes unstable for $f_A, f_B > 2$ in the region where the concentrations c_{s_A} and c_{s_B} of A - and B -stickers roughly match, $c_{s_A} \approx c_{s_B}$.

Excluded volume interactions can restore the stability. For $v > 0$ and $c_{s_A} \approx c_{s_B} \approx c_s/2$, the determinant is

$$\det(H_f)|_{K \rightarrow 0} \approx \frac{2}{|c_{s_A} - c_{s_B}|} \left[-\frac{1 - \frac{1}{f_A} - \frac{1}{f_B}}{c_s} + \frac{1}{2} v \left(\left(\frac{N_A}{f_A} + \frac{N_B}{f_B} \right)^2 - 2 \right) \right], \quad (16)$$

where we have omitted terms that do not scale like $1/|c_{s_A} - c_{s_B}|$. This equation shows that the excluded volume interactions can stabilize the homogeneous state at higher concentrations. The effect increases with increasing spacer content in the system, i.e., large values of N_i/f_i . Nevertheless, the system will remain unstable at low concentrations, i.e., $c_s \rightarrow 0$ as long as $K \rightarrow 0$, i.e., at infinite binding strength.

If the binding strength is finite, bond formation is suppressed in the very dilute regime for entropy reasons, which also restores stability. For $K > 0$ and $v = 0$, the determinant of the Hesse matrix for small total sticker concentration c_s reads

$$\det(H_f)|_{v=0} = \frac{1}{c_{s_A} c_{s_B}} \left[\frac{1}{f_A f_B} + \frac{1 - \frac{1}{f_A} - \frac{1}{f_B}}{2} \times \left(1 - \frac{K + c_s}{\sqrt{(K + c_s)^2 - 4c_{s_A} c_{s_B}}} \right) \right] \approx \frac{1}{f_A f_B c_{s_A} c_{s_B}} - \frac{1 - \frac{1}{f_A} - \frac{1}{f_B}}{K^2} + \mathcal{O}(c_s). \quad (17)$$

For sufficiently large dissociation constant K , the instability at small concentrations is thus removed.

In order to apply the theory to the simulation model, we must determine the excluded volume parameter v . This parameter, also known as the second virial coefficient, is calculated using the Mayer-f function:

$$v_{\text{ex}} = 2\pi \int_0^\infty dr r^2 \left(1 - e^{-\beta w(r)} \right). \quad (18)$$

Here, $\beta w(r)$ represents the nonbonded monomer-monomer interaction potential, i.e., the WCA potential (Eq. (2)). Substituting the WCA potential in Eq. (18), we obtain $v = 2.2\sigma^3$. Inserting this value and $\varepsilon_{\text{sp}} = 6k_B T$, we find that the determinant of the Hesse matrix is always positive in our system, indicating that the homogeneous state is stable or at least metastable. A numerical evaluation of f (Eq. (12)) suggests that the homogeneous phase is truly stable. Therefore, the theory predicts that our system should not exhibit phase separation.

We emphasize that this is not a general result, but a feature of the system studied in the present work. The Semenov-Rubinstein theory of associative polymer solutions does predict the existence of a phase-separated regime [12, 28, 29]. Danielsen et al. have shown that the extent of this regime is significantly reduced in mixtures of heteroassociative polymers, compared to single-component systems of associative polymers [33]. The considerations above highlight the role of excluded volume interactions between the spacer monomers in suppressing phase separation at high polymer concentrations, in agreement with arguments by Harmon et al. [12], and the role of the finite binding strength in suppressing phase separation at low polymer concentrations.

To verify the theoretical prediction in simulations, we focus on the case $c_{s_A} = c_{s_B}$ where instabilities are most

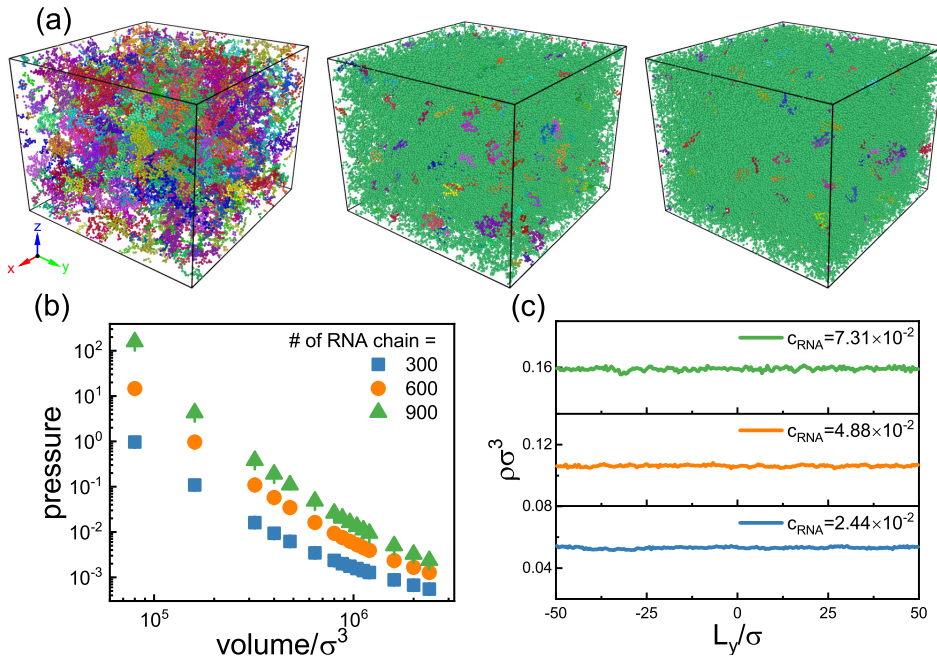


FIG. 3. (a) Snapshots of the system for different RNA monomer concentrations in the equilibrium state (Left to right: $c_{\text{RNA}} = 2.44 \times 10^{-2} \sigma^{-3}$, $4.88 \times 10^{-2} \sigma^{-3}$, $7.31 \times 10^{-2} \sigma^{-3}$). Multi-colored particles belong to different clusters. (b) Pressure-volume graph for different numbers of RNA chains. In each case, the ratio of RNA and trimer chains is fixed at $n_{\text{RNA}}/n_{\text{trimer}} = 3/10$, such that the total numbers of stickers of RNA and trimers match each other. (c) Average density profile along y direction for each case in the volume $8 \times 10^5 \sigma^3$.

likely to occur in the homogeneous mixture. Therefore, we set the ratio of A -chains (RNA) to B -chains (trimers) to $n_A/n_B = 3/10$, such that $f_{ANA} = f_{BNB}$. Fig. 3(a) shows snapshots of our system in the equilibrium state for three different polymer concentrations. Polymers belonging to different clusters are colored differently. With increasing concentration, RNA and trimer chains bind together to form larger clusters. At low concentrations, (RNA bead concentration $c_{\text{RNA}} = 2.44 \times 10^{-2} \sigma^{-3}$), small clusters are uniformly dispersed throughout the system (see Fig. 3(a), left panel), whereas at higher concentrations, a single connected cluster spans the whole system (Fig. 3(a), middle and right panel). Nevertheless, no phase separation occurs. To demonstrate this, we utilize two kinds of verification methods. According to thermodynamics, phase separation is associated with a plateau in a graph of pressure versus the volume at fixed molecule number. In small systems, this plateau could be replaced by nonmonotonic behavior (a van-der-Waals loop). Fig. 3(b) shows the pressure-volume relationships for three different values of polymer numbers. The pressure decreases monotonously with increasing volume, with no signature of unusual behavior at any concentration. Alternatively, inspecting the density profile offers another method to investigate the phase behavior directly. This method is often utilized in recent research [47, 48]. The density profiles along the y -direction are shown in Fig. 3(c). They are nearly uniform, with no sign of large density variations as would be characteristic for phase separation.

In summary, the findings from the two methods strongly support the theoretical result that our current system does not experience phase separation. However, this is not a generic property of our model. If we reduce the spacer length, i.e., reduce N_i/f_i , the system exhibits a phase-separated region both according to theory and simulations. This case will be discussed elsewhere.

III.B Sol-gel transition

As discussed in Section II.B and in the literature[29, 49], systems of associative polymers may exhibit a percolation transition. We recall that the term percolation denotes a geometrical transition in an infinite system of partially connected units (polymers) between a state where all connected clusters are finite to a state where a large system-spanning cluster exists. Thus, the notion of "percolation" depends on the definition of connectivity in a cluster. In many computational studies and cluster algorithms, molecules are taken to belong to the same cluster if they satisfy certain proximity criteria, e.g., the minimum distance between monomers in the two chains is below a given threshold value. Here, following the spirit of the Semenov-Rubinstein theory, we take two chains to be connected if a specific bond has formed between them. Due to the high energy of specific interactions, the existence of an infinite cluster then also implies a change in

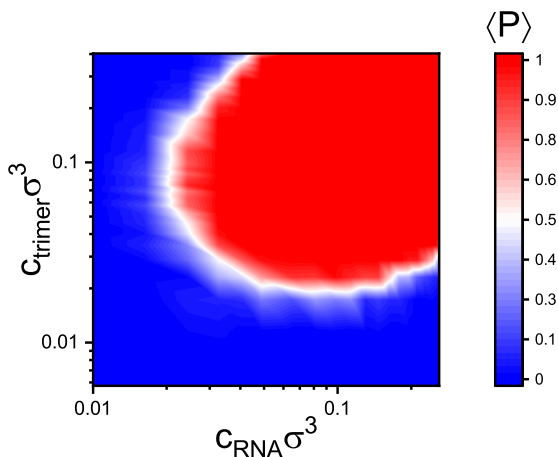


FIG. 4. Order parameter $\langle P \rangle$ with different concentrations of RNA and trimers. In the red region, a percolation transition occurs, with the white line indicating the percolation threshold.

rheological properties and the emergence of rubber-like behavior on sufficiently short time scales, as is characteristic for a sol-gel transition.

Percolation is a sharp and well-defined transition in the thermodynamic limit, where the spanning cluster is infinitely large. In finite homogeneous systems, the transition smoothens, but it can still be characterized in terms of spanning clusters. Since we use periodic boundary conditions in our simulations, we can define a spanning cluster through the requirement that a closed path within the cluster can be traced from any particle to its periodic image. Based on this definition, we define an order parameter for the percolation transition P via

$$P = \begin{cases} 1 & : \text{configuration contains } \geq 1 \text{ spanning clusters} \\ 0 & : \text{otherwise} \end{cases} \quad (19)$$

and we calculate the time-averaged value of this quantity, $\langle P \rangle$, in the equilibrated systems. Since we consider reversible binding, this corresponds to a statistical average with Boltzmann weight. In infinite systems, the percolation transition is characterized by a jump from $\langle P \rangle = 0$ to $\langle P \rangle = 1$. In finite systems, the jump is replaced by a continuous, but quite sharp transition. This is because the probability to sample a configuration with $P = 0$, i.e., a configuration without spanning clusters, is never strictly zero in finite systems, and the same holds for $P = 1$ if the number of chains in the system is high enough that they can form a spanning cluster. Fig. 4 shows the behavior of $\langle P \rangle$ in our system for different concentrations of RNA and trimers and thus traces out the phase diagram of the percolation transition.

The figure demonstrates one striking feature of our system: For fixed RNA or trimer concentration, increasing the concentration of the other component leads to reentrant behavior. For example, at fixed trimer bead concentration $c_{\text{trimer}} \sim 0.03\sigma^{-3}$, percolation sets in once the

RNA bead concentration reaches $c_{\text{RNA}} \sim 0.03\sigma^{-3}$, but is suppressed again at $c_{\text{RNA}} > 0.25\sigma^{-3}$. Likewise, at fixed RNA bead concentration $c_{\text{RNA}} \sim 0.03\sigma^{-3}$, percolation is only observed in a window of trimer bead concentrations, $0.03\sigma^{-3} < c_{\text{trimer}} < 0.23\sigma^{-3}$. Summarizing the results shown in Fig. 3 and 4, we conclude that specific binding in our RNA-trimer system induces a percolation transition without phase separation if the concentrations of the components reach a certain threshold, but are not too much in excess of each other.

We will now set out to compare the simulation results with the theory of Section II.B. We start with considering the average fraction of bound RNA and trimer stickers, p_A and p_B , which are calculated according to Eq. (11). Fig. 5 shows the corresponding density of bound sticker pairs, i.e., the total number of specific bonds per volume, N_p/V , for different RNA and trimer concentrations, as obtained from simulations and predicted by theory. The theory agrees remarkably well with the simulations especially at high concentrations, see Fig. 5 (d), even though it has no adjustable parameters. The largest discrepancies are observed at small trimer and RNA concentrations, where the theory overestimates the binding numbers.

As we have discussed earlier, central mean-field assumptions in the Semenov-Rubinstein theory are that excluded volume interactions are small on the spacer scale that spacers overlap. This results in the conditions $v \cdot l > v_l$ and $c_{si} < 1/v_l$ for $i = A$ or B , where v_l denotes the volume covered by a spacer. It has been approximated as [33] $v_l \sim (a\sqrt{l})^3$, or, slightly more sophisticated [50], as $v_l \sim \frac{4}{3}\pi(a\sqrt{l})^3$. In our system, the parameters are $a \sim 1.2\sigma$, $v \sim 2.2\sigma^3$ and $l_A = 5$, $l_B = 10$. Hence, we have $v \cdot l \sim 11\sigma^3$ for RNA and $v \cdot l \sim 22\sigma^3$ for trimers, which must be compared to $v_l \sim 19\sigma^3$ or $\sim 81\sigma^3$ for RNA and $v_l \sim 55\sigma^3$ or $\sim 229\sigma^3$ for trimer, depending on the estimate. Since $v \cdot l < v_l$, excluded volume effects can be considered small. On the other hand, the spacer overlap concentration is $1/v_l \sim 0.05\sigma^{-3}$ or $\sim 0.01\sigma^{-3}$ for RNA, and $1/v_l \sim 0.02\sigma^{-3}$ or $\sim 0.004\sigma^{-3}$ for trimers, depending on the estimate. The first estimate corresponds to $c_{\text{RNA}} \sim 0.34\sigma^{-3}$ and $c_{\text{trimer}} \sim 0.14\sigma^{-3}$, which is higher than most concentrations considered in the present study. The second estimate corresponds to $c_{\text{RNA}} < 0.08\sigma^{-3}$ and $c_{\text{trimer}} < 0.03\sigma^{-3}$, which is comparable to our values at intermediate RNA and trimer concentrations. Thus we conclude that most of our systems are in the dilute regime, or on the verge of being dilute, which explains the discrepancies between theory and simulations at low concentrations. The mean-field theory also assumes that the number of stickers on a chain is large $f \gg 1$, which is clearly not true in the case of the trimers. However, this factor seems to be less important. At higher concentrations, the theoretical predictions for the binding density are in almost quantitative agreement with the simulation results.

Next we consider the percolation transition. From the data shown in Fig. 4, we determine the percola-

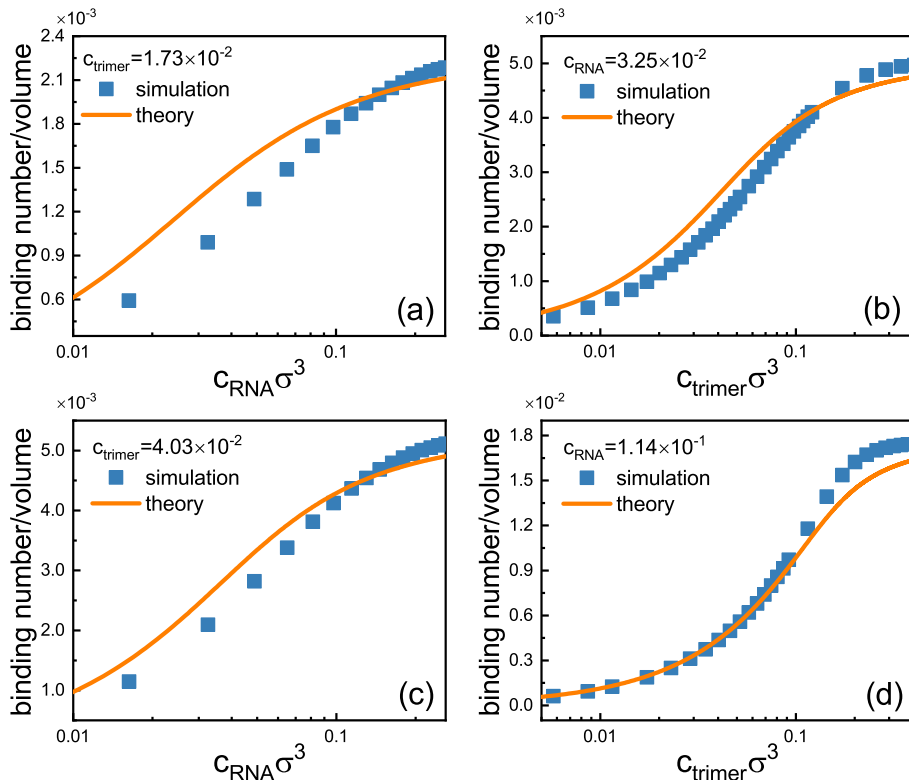


FIG. 5. Density of specific bonds in the simulations (a,c) as a function of RNA concentration for fixed trimer concentrations as indicated and (b,d) as a function of trimer concentration for fixed RNA concentrations as indicated. Blue square symbols show the results of the simulation. Orange solid lines are the results based on Eq. (10) using the same parameters as in our simulation.

tion threshold as the point where $\langle P \rangle = 0.5$. In other studies[28], a fitting function was utilized to estimate the percolation threshold. We tested that procedure for some cases and found the discrepancy between this method and ours to be small. We also checked that the results are not strongly affected by finite-size effects, indicating that the simulation box is large enough[51].

Fig. 6 shows the simulation data for the percolation transition according to the definition above along with the theoretical prediction of Eq. (13). This equation relates the percolation threshold with the fractions p_{RNA} and p_{trimer} of bound RNA and trimer stickers, respectively, which are in turn calculated from Eq. (11). The theory predicts that the polymer network should percolate if the average number of trimer-mediated connections between RNA-chains, $m = 18 p_{\text{RNA}} p_{\text{trimer}}$, exceeds the threshold $m_p = 1$. This prediction, shown as orange line in Fig. 6(a), greatly overestimates the concentration region where percolation is observed. However, as we have argued in Section II.B, $m_p = 1$ just gives lower bound for the onset of percolation. The true threshold value m_p should be larger, for example, due to the existence of closed paths (cycles) in the percolating cluster. If we treat the threshold value as adjustable parameter and increase it to $m_p = 2$, the area of the percolated

regime in the $C_{\text{RNA}}-C_{\text{trimer}}$ plane shrinks, but the shape of the percolated phase is still not captured well by the theory, especially at low RNA concentrations.

On the other hand, we recall that this low concentration regime is precisely the one where the theoretical predictions for the binding numbers deviate from the simulation results (see Fig. 5). Therefore, as a remedy, we also test the prediction of Eq. (13) if the values for bound sticker fractions p_{RNA} and p_{trimer} are taken from the simulations. The corresponding curves are shown as solid lines in Fig. 6(b), again together with the simulation results for the percolation transition. One can see that the theoretically predicted shape of the percolated region captures the shape according to simulations much better. Assuming the threshold value of m to be at $m_p = 1$, the size of the percolated region is still too large, but we obtain reasonable agreement for $m_p \approx 2.5$.

As we have argued previously, one possible reason for the deviation – even when using the binding numbers from the simulation in Eq. (13) – is the presence of cycles in the percolation cluster of the real system. To investigate the effects of cycles, we have identified, in each configuration, the minimal bonds necessary to maintain the connectivity of all clusters and removed all the others, thus removing all cycles in the system. This

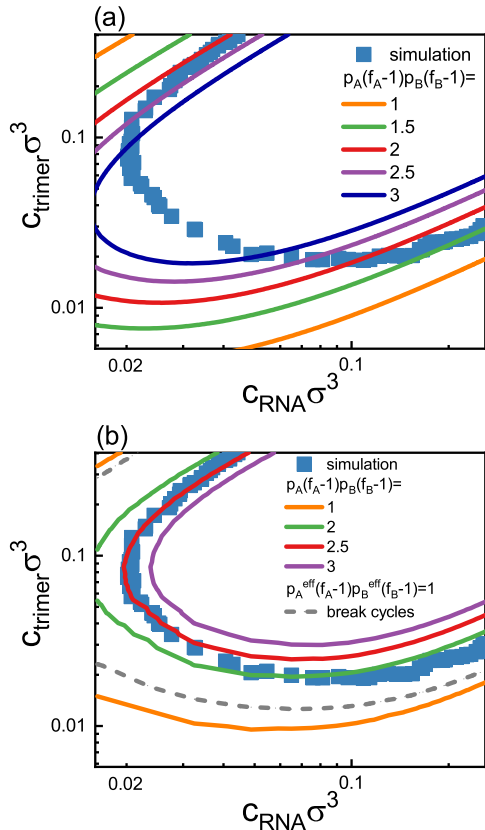


FIG. 6. Comparison of percolation threshold between the simulation and theory. Blue square symbols are the results of the simulation. Solid lines are the theoretical predictions based on Eq. (13) for different values of the threshold value m_c as indicated and binding fractions p_i taken from (a) theory (Eq. (11)) and (b) simulations. The gray dash line shows the modification for $p_A(f_A - 1)p_B(f_B - 1) = 1$. In this case, we break all cycles (remain only one cycle for the spanning cluster) but keep cluster connectivity in the entire system.

was done using the NetworkX Python package[52] and Kruskal’s algorithm[53]. In the gray dashed line in Fig. 6(b), we compare the results obtained for $m_p = 1$ after removing the cycles (except for one cycle for the spanning cluster) with the simulation results. Here, the input parameter is the effective binding probability $p_i^{\text{eff}} = (N_p - N_{\text{break cycles}}^{\text{max}})/n_i f_i$, where $N_{\text{break cycles}}^{\text{max}}$ is the maximal number of bonds that could be removed to break cycles without destroying clusters. This adjustment brought the theoretically predicted percolation line closer to that obtained in the simulations, however, the theory still substantially underestimates the percolation threshold. Thus the presence of cycles does not seem to be the primary cause of the deviation.

To summarize, the mean-field theory can predict the binding number fairly well, especially in dense solutions, but the predicted percolation threshold deviates strongly from the threshold located in the simulations. This de-

viation can partly be attributed to inaccuracies in the prediction for the binding number at small RNA concentrations, and partly to the fact that the theory assumes a tree-like graph structure of the percolating cluster at the transition and neglects the possibility of cycles. However, these two effects cannot fully explain the disagreement between theory and simulations. The theory underestimates the number of bonds needed to create a percolating cluster. Interestingly, good agreement between theory and simulations can be obtained if this number is treated as a single adjustable parameter.

III.C Analysis of binding structures

Finally, we examine in more detail the molecular basis of the reentrance behavior in the percolation, which is predicted by theory[33] and observed in Fig. 4. To this end, we define three binding structures: bridges, loops, and “binding only once” (see cartoon in Fig. 7(e)). A bridge is formed when two stickers on a trimer bind to two different RNA chains. A loop occurs when two stickers on a trimer attach to the same RNA chain. A trimer can be part of one or several bridges, or loops, or both. If only one of its stickers is bound, it is classified as “binding only once”. Additionally, the relative mass of the spanning cluster ϕ is defined as the ratio of the number of particles in the spanning cluster to the total number of particles in the system. We utilize the freud-analysis package[54] to perform the cluster analysis. Fig. 7 shows the details of the spanning cluster and the binding structures for two cases.

Fig. 7(a) and (c) focus on the behavior of the system at fixed trimer concentration as a function of RNA concentration. If the RNA concentration is low ($C_{\text{RNA}} = 1.63 \times 10^{-2}\sigma^{-3}$), the number of bridges is lower than that of loops, with the majority of trimers being attached to only one RNA sticker. Thus, forming a spanning cluster is challenging. As the RNA bead concentration increases beyond $C_{\text{RNA}} > 0.06\sigma^{-3}$, RNA and trimers connect to spanning clusters, where bridges outnumber loops. However, the total fraction of monomers in the largest cluster never exceeds 80 percent. Further adding RNA reduces the spanning cluster’s relative mass until percolation breaks down at $C_{\text{RNA}} = 0.26\sigma^{-3}$. In this reentrance region, the number of bridges and loops both reach saturation, as all trimer binding sites become occupied. The total number of specific bonds in the system saturates (cf. Fig. 5(a,c)). As a consequence, the fraction p_{RNA} of occupied RNA sticker sites subsequently decreases with increasing RNA concentration, which, by virtue of Eq. (13), leads to a reduction of the average number of trimer-mediated connections between RNA molecules and reduces the percolation probability. At large RNA content, most RNA molecules only bind to one trimer. Even though trimers still preferably form bridges between RNA, the number of bridges is not sufficient to create a percolating network.

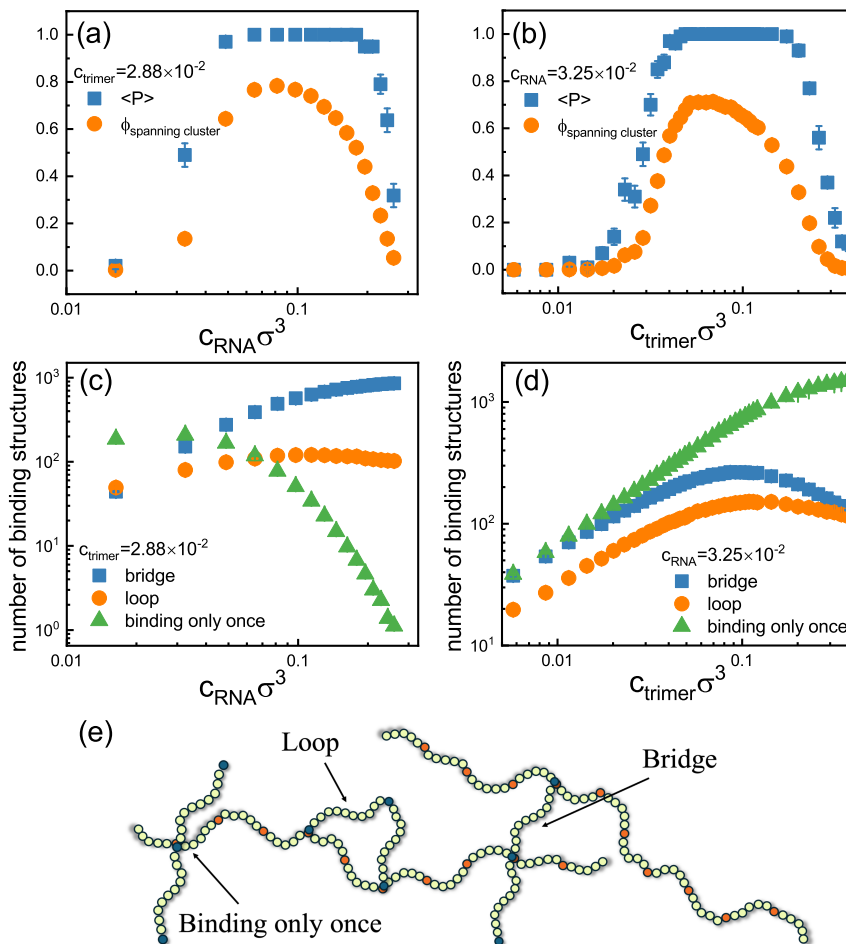


FIG. 7. (a,b) Order parameter $\langle P \rangle$ (blue squares) and size of spanning cluster ϕ (orange circles) in the case of fixed trimer bead concentration $c_{\text{trimer}} = 2.88 \times 10^{-2} \sigma^{-3}$ and fixed RNA bead concentration $c_{\text{RNA}} = 3.25 \times 10^{-2} \sigma^{-3}$. (c,d) Corresponding number of binding structures. (e) Snapshot for three binding structures as defined in the main text.

Owing to the structural similarity, the same reentrance behavior can be observed at fixed RNA concentration, as shown in Fig. 7(b) and (d). Increasing the trimer concentration initially facilitates percolation, and the spanning cluster size and bridge number reach a maximum at trimer concentration $c_{\text{trimer}} = 6 \times 10^{-2} \sigma^{-3}$. However, adding excess trimers to the system subsequently leads to a situation where all binding sites in RNA are occupied by different trimers, so that the number of trimers that bind only once keeps increasing, while the numbers of bridges and loops decrease. The reorganization of binding structures eventually inhibits the formation of spanning clusters.

To further analyze this phenomenon, we calculated the histogram of cluster size distributions. Here, we average the histogram over time. The results are shown in Fig. 8. At fixed trimer concentration $c_{\text{RNA}} = 3.25 \times 10^{-2} \sigma^{-3}$ (top panel in (a)), the system does not contain enough RNA molecules to form a spanning cluster, hence the contribution of clusters containing more than 2×10^4 particles is not significant. In the percolation region, clusters of

intermediate size (containing 3×10^3 to 2×10^4 particles) decrease in number and merge into larger clusters. As the RNA concentration continues to increase, the system again predominantly forms smaller clusters, and at $c_{\text{RNA}} = 2.44 \times 10^{-1} \sigma^{-3}$ (bottom panel in (a)), large clusters become rare. Fig. 8(b) shows the evolution of cluster size distributions for fixed $c_{\text{RNA}} = 3.25 \times 10^{-2} \sigma^{-3}$. Here, adding more trimers leads to the formation of more bridges that recruit RNA into the large clusters, such that the largest cluster size exceeds 2×10^4 particles (middle panel in (b)). However, adding further trimers results in a dominance of "single binding" instances, causing the large clusters to break into several smaller clusters (bottom panel in (b)). In summary, increasing the concentration of one component can lead to reentrant behavior in the phase diagram. The size of the largest cluster decreases, and eventually, percolation is no longer observed. If the trimers are in excess, this is associated with a reorganization of binding structures as described above, such that the bridges lose their dominant role. If RNA is in excess, the bridges remain

dominant, but the number of bridges per RNA molecule is too small to sustain percolation. The results suggest that there exist two cluster populations in the percolation region: one population with a size distribution that decreases roughly exponentially as a function of cluster size, and one featuring a distinct peak at a large, "macroscopic" cluster size. Outside the percolation region, the latter peak disappears and all cluster sizes are exponentially distributed. Therefore, the existence of this peak might be a good alternative criterion that could be used to identify percolation transitions in real finite systems, where the spanning cluster criterion cannot be applied.

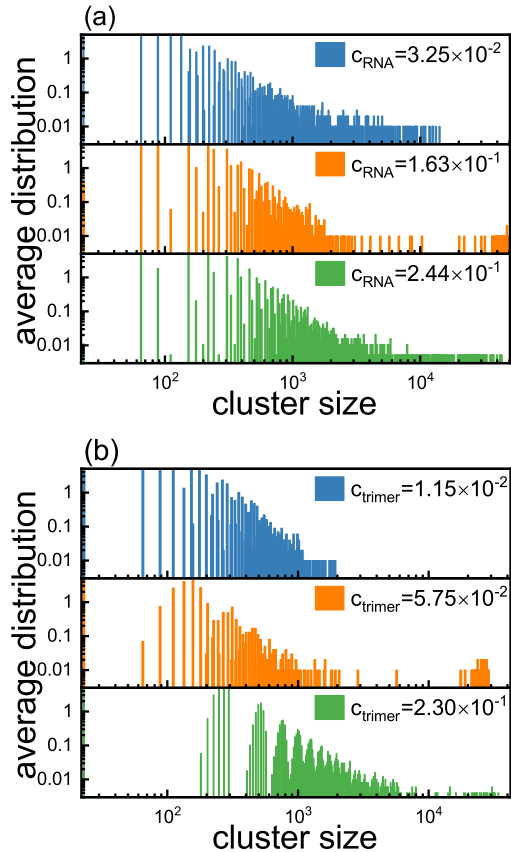


FIG. 8. Distribution of cluster sizes for the case fixed trimer concentrations $c_{\text{trimer}} = 2.88 \times 10^{-2} \sigma^{-3}$ (a) and fixed RNA concentrations $c_{\text{RNA}} = 3.25 \times 10^{-2} \sigma^{-3}$ (b), respectively.

IV SUMMARY

The main purpose of the present study was to investigate the impact of specific binding on the phase behavior of heteroassociative polymer solutions, such as solutions of RNA and proteins containing domains that can selectively bind to RNA. To this end, we have utilized molecular dynamics simulation to study the percolation transition without phase separation in RNA-protein mixtures,

and compared the results with the mean-field theory of associative polymers. Our main results can be summarized as follows:

- (1) Percolation can be observed in heteroassociative mixtures if the concentration of both components is sufficiently high. In the systems considered in the present work, the percolation was not accompanied by liquid-liquid phase separation.
- (2) The percolation phase diagram features double reentrance behavior with increasing each concentration of either the RNA or the protein component. Protein mediated bridge formation is identified as being crucial for cluster formation and the percolation transition. If one of the two components is in excess of the other, percolation is suppressed: If proteins are in excess, bridges do not form. If RNA is in excess, the number of bridges per RNA molecule is not sufficient. In both cases, this inhibits percolation.
- (3) The mean field theory for associative polymer can be extended to two asymmetric components and can be used to predict the behavior of the RNA-protein system. The theory successfully captures the evolution of binding numbers as a function of the concentrations of the two components, especially at high concentrations, and explains the stability of the homogeneous system. It shows how spacers between binding sites on the RNA and the proteins play a crucial role in modulating the competition between specific and unspecific monomer interactions, thereby enhancing the solubility of each component and preventing phase separation in our system. However, the theory fails to accurately predict the percolation threshold. This discrepancy can be attributed in part to small deviations between the average number of specific bonds as obtained from simulations and theory due to the fact that the concentrations of the polymers are in a regime where the conditions for the validity of the mean-field theory are not fulfilled. Another factor is the existence of closed, paths in the percolating cluster at the percolation threshold, which is neglected by the theory. However, our detailed analysis shows that these two factors cannot fully account for the discrepancy between theory and simulations. Interestingly, good agreement between theory and simulations can be obtained by introducing a single heuristic fit parameter into the criterion for the percolation threshold.

Previous studies have often focused on the phase separation behavior of biomolecular systems. The present paper enhances the understanding of the mechanisms underlying the formation of percolating networks involving RNA and proteins. For proteins, many factors control the phase behaviors, such as the sequence of IDRs and RBDs, the solubility of IDRs, the binding specifics of RBDs, etc. In our study, we only discussed the effect of specific binding between RBDs of proteins and RNA, and we did this

at a very generic level. We did not consider the impact of nonspecific binding, which may lead to the formation of metastable, long-living droplets in sticker-spacer models for proteins according to the literature[13]. Moreover, we used a simple simulation model of fully flexible chains and did not consider possible effects of chain rigidity, e.g., of RNA. Another interesting topic for future studies is sequence-dependent gelation or phase separation. For example, Jain and Vale found that RNA with longer repeats(GGGGCC) formed an interconnected mesh-like network, while RNA with different repeats(CCCCGG) was soluble[55]. Seim et al. reported that for a fungal RNP protein, Whi3, the formation of transient alpha-helical structures also modulates phase separation by promoting the assembly of dilute phase oligomers[56]. According to this literature, the sequence of the special binding motif in RNA or proteins also emerges as a crucial determinant in determining the phase transitions in the system.

We have shown that the Semenov-Rubinstein theory provides reasonable predictions of the behavior of associative polymers in the semidilute regime, but it cannot capture correlations in the dilute regime, where stickers

are no longer evenly distributed in the system. Moreover, it neglects the conformational entropy of chains. Recently, Rovigatti et al. studied the role of entropy in the phase behavior of systems of associating single-chain nanoparticles[57] and showed that the configurational and combinatorial binding entropy can modulate the phase behavior.

In summary, our approach provides basic insights into the unique phase behaviors of RNA-protein systems driven by specific binding, setting the stage for more detailed investigations into the factors governing these phenomena including their theoretical description.

ACKNOWLEDGMENTS

This project was funded by SFB 1551 Project No. 464588647 of the DFG (Deutsche Forschungsgemeinschaft). The authors gratefully acknowledge the computing time provided to them on the high-performance computer Mogon2 and Mogon NHR South-West.

-
- [1] A. A. Hyman, C. A. Weber, and F. Jülicher, Annual review of cell and developmental biology **30**, 39 (2014).
 - [2] S. F. Banani, H. O. Lee, A. A. Hyman, and M. K. Rosen, Nature reviews Molecular cell biology **18**, 285 (2017).
 - [3] C. P. Brangwynne, C. R. Eckmann, D. S. Courson, A. Rybarska, C. Hoegge, J. Ghatakani, F. Jülicher, and A. A. Hyman, Science **324**, 1729 (2009).
 - [4] F. Bolognani and N. I. Perrone-Bizzozero, Journal of neuroscience research **86**, 481 (2008).
 - [5] V. O. Wickramasinghe and A. R. Venkitaraman, Molecular cell **61**, 496 (2016).
 - [6] Y. Shi, Nature reviews Molecular cell biology **18**, 655 (2017).
 - [7] A. S. Rahmanto, C. J. Blum, C. Scalera, J. B. Heideberger, M. Mesitov, D. Horn-Ghetko, J. F. Gräf, I. Mikić, R. Hobrecht, A. Orekhova, *et al.*, Molecular Cell **83**, 4272 (2023).
 - [8] S. Poblete, A. Bozic, M. Kanduc, R. Podgornik, and H. V. Guzman, ACS omega **6**, 32823 (2021).
 - [9] Y. Lin, D. S. Protter, M. K. Rosen, and R. Parker, Molecular cell **60**, 208 (2015).
 - [10] S. Maharana, J. Wang, D. K. Papadopoulos, D. Richter, A. Pozniakovsky, I. Poser, M. Bickle, S. Rizk, J. Guillén-Boixet, T. M. Franzmann, *et al.*, Science **360**, 918 (2018).
 - [11] A. Mollieux, J. Temirov, J. Lee, M. Coughlin, A. P. Kanagaraj, H. J. Kim, T. Mittag, and J. P. Taylor, Cell **163**, 123 (2015).
 - [12] T. S. Harmon, A. S. Holehouse, M. K. Rosen, and R. V. Pappu, elife **6**, e30294 (2017).
 - [13] S. Ranganathan and E. I. Shakhnovich, Elife **9**, e56159 (2020).
 - [14] E. Jankowsky and M. E. Harris, Nature reviews Molecular cell biology **16**, 533 (2015).
 - [15] M. Garcia-Jove Navarro, S. Kashida, R. Chouaib, S. Souquere, G. Pierron, D. Weil, and Z. Gueroui, Nature communications **10**, 3230 (2019).
 - [16] E. W. Martin and A. S. Holehouse, Emerging topics in life sciences **4**, 307 (2020).
 - [17] M. W. Hentze, A. Castello, T. Schwarzl, and T. Preiss, Nature reviews Molecular cell biology **19**, 327 (2018).
 - [18] F. Gebauer, T. Schwarzl, J. Valcárcel, and M. W. Hentze, Nature Reviews Genetics **22**, 185 (2021).
 - [19] C. Roden and A. S. Gladfelter, Nature Reviews Molecular Cell Biology **22**, 183 (2021).
 - [20] S. Boeynaems, A. S. Holehouse, V. Weinhardt, D. Kovacs, J. Van Lindt, C. Larabell, L. Van Den Bosch, R. Das, P. S. Tompa, R. V. Pappu, *et al.*, Proceedings of the National Academy of Sciences **116**, 7889 (2019).
 - [21] H. Zhang, S. Elbaum-Garfinkle, E. M. Langdon, N. Taylor, P. Occhipinti, A. A. Bridges, C. P. Brangwynne, and A. S. Gladfelter, Molecular cell **60**, 220 (2015).
 - [22] J. Kang, L. Lim, Y. Lu, and J. Song, PLoS biology **17**, e3000327 (2019).
 - [23] C. P. Brangwynne, P. Tompa, and R. V. Pappu, Nature Physics **11**, 899 (2015).
 - [24] D. S. Protter, B. S. Rao, B. Van Treeck, Y. Lin, L. Mizoue, M. K. Rosen, and R. Parker, Cell reports **22**, 1401 (2018).
 - [25] S. Qamar, G. Wang, S. J. Randle, F. S. Ruggeri, J. A. Varela, J. Q. Lin, E. C. Phillips, A. Miyashita, D. Williams, F. Ströhl, *et al.*, Cell **173**, 720 (2018).
 - [26] S. Alberti, A. Gladfelter, and T. Mittag, Cell **176**, 419 (2019).
 - [27] J.-M. Choi, F. Dar, and R. V. Pappu, PLoS computational biology **15**, e1007028 (2019).
 - [28] J.-M. Choi, A. A. Hyman, and R. V. Pappu, Physical Review E **102**, 042403 (2020).
 - [29] A. N. Semenov and M. Rubinstein, Macromolecules **31**,

- 1373 (1998).
- [30] W. Borchers, A. Bremer, M. B. Borgia, and T. Mittag, *Current opinion in structural biology* **67**, 41 (2021).
- [31] J. R. Espinosa, J. A. Joseph, I. Sanchez-Burgos, A. Garaizar, D. Frenkel, and R. Collepardo-Guevara, *Proceedings of the National Academy of Sciences* **117**, 13238 (2020).
- [32] J. A. Joseph, J. R. Espinosa, I. Sanchez-Burgos, A. Garaizar, D. Frenkel, and R. Collepardo-Guevara, *Biophysical Journal* **120**, 1219 (2021).
- [33] S. P. O. Danielsen, A. N. Semenov, and M. Rubinstein, *Macromolecules* **56**, 5661 (2023).
- [34] A. M. Krecic and M. S. Swanson, *Current opinion in cell biology* **11**, 363 (1999).
- [35] A. Decorsière, A. Cayrel, S. Vagner, and S. Millevoi, *Genes & development* **25**, 220 (2011).
- [36] P. Herviou, M. Le Bras, L. Dumas, C. Hieblot, J. Gilhodes, G. Cioci, J.-P. Hugnot, A. Ameadan, F. Guillonneau, E. Dassi, *et al.*, *Nature communications* **11**, 2661 (2020).
- [37] J. D. Weeks, D. Chandler, and H. C. Andersen, *The Journal of chemical physics* **54**, 5237 (1971).
- [38] Y. Zhang, B. Xu, B. G. Weiner, Y. Meir, and N. S. Wingreen, *Elife* **10**, e62403 (2021).
- [39] T. GrandPre, Y. Zhang, A. G. Pyo, B. Weiner, J.-L. Li, M. C. Jonikas, and N. S. Wingreen, *PRX Life* **1**, 023013 (2023).
- [40] J. A. Anderson, C. D. Lorenz, and A. Travesset, *Journal of computational physics* **227**, 5342 (2008).
- [41] A. Stukowski, *MODELLING AND SIMULATION IN MATERIALS SCIENCE AND ENGINEERING* **18** (2010), 10.1088/0965-0393/18/1/015012.
- [42] N. Galvanetto, M. T. Ivanović, A. Chowdhury, A. Sottini, M. F. Nüesch, D. Nettels, R. B. Best, and B. Schuler, *Nature* **619**, 876 (2023).
- [43] D. Prusty, V. Pryamitsyn, and M. Olvera de la Cruz, *Macromolecules* **51**, 5918 (2018).
- [44] J. J. Michels, M. Brzezinski, T. Scheidt, E. A. Lemke, and S. H. Parekh, *Biomacromolecules* **23**, 349 (2021).
- [45] P. J. Flory, *Principles of polymer chemistry* (Cornell university press, 1953).
- [46] W. H. Stockmayer, *The Journal of chemical physics* **11**, 45 (1943).
- [47] Z. Benayad, S. von Bülow, L. S. Stelzl, and G. Hummer, *Journal of Chemical Theory and Computation* **17**, 525 (2020).
- [48] S. Rekhi, D. Sundaravadevelu Devarajan, M. P. Howard, Y. C. Kim, A. Nikoubashman, and J. Mittal, *The Journal of Physical Chemistry B* **127**, 3829 (2023).
- [49] X. Zeng and R. V. Pappu, *Current Opinion in Structural Biology* **79**, 102540 (2023).
- [50] M. Doi and S. Edwards, *Theory of Polymer Dynamics* (Oxford University Press, New York, 1986).
- [51] G. Wang, A. Zippelius, and M. Müller, *Macromolecules* **55**, 5567 (2022).
- [52] A. A. Hagberg, D. A. Schult, and P. J. Swart, in *Proceedings of the 7th Python in Science Conference*, edited by G. Varoquaux, T. Vaught, and J. Millman (Pasadena, CA USA, 2008) pp. 11 – 15.
- [53] J. B. Kruskal, *Proceedings of the American Mathematical society* **7**, 48 (1956).
- [54] V. Ramasubramani, B. D. Dice, E. S. Harper, M. P. Spellings, J. A. Anderson, and S. C. Glotzer, *Computer Physics Communications* **254**, 107275 (2020).
- [55] A. Jain and R. D. Vale, *Nature* **546**, 243 (2017).
- [56] I. Seim, A. E. Posey, W. T. Snead, B. M. Stormo, D. Klotsa, R. V. Pappu, and A. S. Gladfelter, *Proceedings of the National Academy of Sciences* **119**, e2120799119 (2022).
- [57] L. Rovigatti and F. Sciortino, *Physical Review Letters* **129**, 047801 (2022).